Ab initio study of structural and electronic properties and hyperfine interactions at the Ta nucleus in Ta-doped monoclinic HfO_2

R. E. Alonso,[1,*] L. A. Errico,[1,2] E. L. Peltzer y Blancá,[3] A. López-García,[1] A. Svane,[4] and N. E. Christensen[4]
[1]*Departamento de Física and Instituto de Física La Plata (IFLP, CCT-La Plata, CONICET-UNLP), Facultad de Ciencias Exactas, Universidad Nacional de La Plata, Casilla de Coreo 67, 1900 La Plata, Argentina*
[2]*Universidad Nacional del Noroeste Bonaerense (UNNOBA), Monteagudo 2772, Pergamino, CP 2700 Buenos Aires, Argentina*
[3]*Grupo de Estudio de Materiales y Dispositivos Electrónicos (GEMyDE) Facultad de Ingeniería, IFLYSIB (CONICET), Universidad Nacional de La Plata, C.C. 67, 1900 La Plata, Argentina*
[4]*Department of Physics and Astronomy, University of Aarhus, DK-8000 Aarhus C, Denmark*
(Received 3 July 2008; revised manuscript received 23 September 2008; published 29 October 2008)

The electronic and structural properties of pure and Ta-doped monoclinic HfO_2 have been examined by means of *ab initio* density-functional calculations. The full-potential linear augmented plane wave plus local orbital (APW+LO) method was used here to treat the electronic structure of the doped system including the atomic relaxations introduced by impurities. The effects of reducing the Ta concentration were simulated by means of periodic arrangements of supercells of increasing size, all containing a single Ta atom. The structural relaxations were calculated for two differently charged impurity states and the electrical-field gradients (EFG) at the site of the Ta impurity were derived. The EFGs, as well as the relaxations, depend on the charge state of the impurity. The analysis was carried out by combining time-dependent perturbed angular correlation experimental results and the theoretical APW+LO calculations.

DOI: 10.1103/PhysRevB.78.165206 PACS number(s): 71.15.−m, 76.80.+y, 71.20.−b

I. INTRODUCTION

Hafnia (HfO_2) is a wide-band semiconductor with a large dielectric constant, which is very similar to zirconia (ZrO_2) in chemical and physical properties. Both oxides form in a monoclinic structure at room temperature, transform to tetragonal structures at moderate temperatures, and to cubic structures at high temperatures. HfO_2 is of great technological interest because of its high melting point, high chemical stability, and large dielectric constant. In various forms and with the addition of small amounts of impurities, it has applications ranging from solid oxide fuel cell electrolytes to catalyst substrates and protective coatings (see, e.g., Refs. 1–5 and references therein). In the last years, HfO_2 has attracted much research attention because of its potential application as an alternative to SiO_2 as a dielectric in microelectronic devices due to its high dielectric constant, wide band gap, and stability on Si.[6,7] More recently, ferromagnetism was discovered in pure HfO_2 thin films, a result of great interest to the field of spintronics.[8] Different mechanisms were proposed in order to explain the observed ferromagnetism: O and Hf vacancies and effects of the surface or the interface with the substrate effects.[8] In all cases, impurities, defects, or surfaces and interfaces can introduce structural distortions in the host lattice and impurity levels in the gap of the semiconductor modifying the electronic structure of the system. One way to measure electronic properties on an atomic scale is to use hyperfine experimental techniques.[9] During the last decades, these techniques, such as nuclear quadrupole resonance (NQR), nuclear magnetic resonance (NMR), Mössbauer spectroscopy (MS), and time-dependent perturbed angular correlations (TDPAC),[9] have been extensively applied to study materials from the point of view of solid-state physics, chemistry, and biology in order to elucidate the microscopic environments of constituent or impurity atoms and the nature of chemical bonding in different kind of molecules and compounds.[10–12] In particular, γ-γ TDPAC provides a high-resolution determination of the EFG tensor at the site of a probe atom (generally an impurity in the system under study), a quantity particularly sensitive to slight local changes in the asymmetry of the electronic charge density around the (impurity) probe.[9] The measured EFG may give structural and electronic information of the system that cannot be obtained by other methods, but the interpretation of such measurements is not straightforward. In fact, interpretation of experimental EFG results involves understanding of chemical differences between the probe atom and the ion replaced by the impurity. The experimental results show that the differences between probes and indigenous atoms are manifested in subtle ways that are not well described by simple models, as already pointed out in Ref. 13.

Local and very accurate information about the system under study, provided by the EFG tensor, can be obtained by comparing experimental results with an accurate calculation of the EFG tensor.[14] In the case of doped systems, for an accurate calculation of the EFG, the electronic configuration of the host, perturbed by the presence of the impurity, has to be determined. This can be done in the framework of the density-functional theory (DFT).[15] In this kind of calculation, electronic and structural effects introduced in the host by the presence of the impurity probe (impurity levels, structural distortions, etc.) can be described without the use of arbitrary suppositions. For such purposes, DFT calculations [using the full-potential linear augmented plane wave plus local orbital (APW+LO) method[16,17]] have been performed. In the last years, some of us have studied Cd (the most common used isotope in TDPAC experiments) in different binary oxides, such as rutile TiO_2 (Refs. 11 and 12) and SnO_2 (Ref. 18), In_2O_3 (Ref. 19), Lu_2O_3 (Ref. 20), and SnO (Ref. 21).

These calculations successfully predicted the EFG at Cd impurity sites and yielded quantitative information about the charge states of the impurities and the lattice relaxation that they induce.

In TDPAC experiments, the second most commonly used radioactive probe is ^{181}Ta, introduced through its parent isotope ^{181}Hf which by β^- decay transforms into an excited nuclear state of ^{181}Ta. Similar to the case of the Cd impurity probe, very few systems were studied using DFT calculations. As far as we know the only EFG calculations at Ta impurity oxides are those reported in Ref. 22 (Ta-doped TiO_2 and SnO_2), Ref. 23 (Ta-doped Al_2O_3), and Ref. 24 (Ta in HfO_2) We can add to this list the results for the electronic structure and EFGs in 2H-TaS_2, $LiTaS_2$, and $SnTaS_2$ obtained by Blaha[25] (in these calculations, Ta is an indigenous atom of the compounds).

The central purpose of this paper is to present and discuss the electronic structure of Ta-doped monoclinic hafnia (m-HfO_2). Here, we study the relationship between the calculated EFG (the key experimental quantity) at the impurity site and the structural relaxations and the character and filling of the impurity state. The results are compared with experimental results and previous calculations.

This paper is organized as follows. In Sec. II, the system under study and the method of calculation are described. In Sec. III, the experimental and theoretical results obtained for pure m-HfO_2 are presented, while the structural and electronic properties of Ta-doped m-HfO_2 follow in Sec. IV. In this section we also discuss the effects of the charge state of the impurity and the Ta concentration on the electronic and structural properties. Finally, Sec. V contains the conclusions.

II. METHOD OF CALCULATION

Ab initio electronic structure calculations were used to determine the self-consistent potential and the charge density, and from these first-principles calculations the hyperfine parameters at a Ta impurity replacing Hf were obtained, taking properly into account the structural and electronic effects introduced by the impurity in the host lattice. First this system was approximated by replacing one Hf atom in the m-HfO_2 unit cell by a Ta atom; i.e., an ordered $Hf_{0.75}Ta_{0.25}O_2$ alloy was considered. In a second scenario and to approximate better HfO_2 with an isolated Ta impurity, we considered a periodically repeated large supercell where a Ta atom replaces a single Hf in the host. From these first-principles calculations we obtained the electric-field gradient tensor corresponding to a Ta nucleus located at a Hf site in the m-HfO_2 lattice.

The EFG is a traceless symmetric tensor of rank 2 whose components, denoted by $V_{i,j}$, are defined by the second derivative (with respect to the spatial coordinates) of the Coulomb potential $V(\mathbf{r})$ created by the charge density surrounding a given nucleus,[9]

$$V_{i,j}(\vec{r}=0) = \left.\frac{\partial^2 V}{\partial x_i\, \partial x_j}\right|_{\vec{r}=0}. \quad (1)$$

TABLE I. Calculated and experimentally determined structural parameters for monoclinic HfO_2. Lattice parameters a, b, and c are in Å and β in degrees. For the calculation of the internal parameters x, y, and z, lattice parameters and angles were fixed at the experimental ones. Experimental data were taken from Ref. 26.

Atom	LDA calculation	GGA calculation	Expt.
A	–	–	5.1170_1
B	–	–	5.1754_2
c	–	–	5.2915_2
β	–	–	99.216_2
x(Hf)	0.277	0.276	0.2755_2
y(Hf)	0.041	0.042	0.0397_1
z(Hf)	0.208	0.208	0.2080_2
x(O1)	0.070	0.069	0.0739_{20}
y(O1)	0.334	0.330	0.3318_{17}
z(O1)	0.343	0.345	0.3466_{17}
x(O2)	0.449	0.4445	0.4489_{20}
y(O2)	0.758	0.758	0.7582_{16}
z(O2)	0.479	0.478	0.4800_{22}

The EFG can be determined straightforwardly once the total charge distribution has been accurately calculated. The eigenvalues of the EFG tensor are denoted as V_{XX}, V_{YY}, and V_{ZZ}, and the conventional choice is $|V_{XX}| \leq |V_{YY}| < |V_{ZZ}|$. Hence, V_{ZZ} is the largest eigenvalue of the EFG tensor and the asymmetry parameter η is a measure of the difference between the two eigenvalues V_{XX} and V_{YY},

$$\eta = \frac{V_{XX} - V_{YY}}{V_{ZZ}}. \quad (2)$$

V_{ZZ} is related to the nuclear quadrupole frequency ω_Q obtained in a TDPAC experiment through[9]

$$\omega_Q = \frac{eQV_{ZZ}}{4I(2I-1)\hbar}. \quad (3)$$

Here Q stands for the largest component of the nuclear quadrupole moment tensor of the sensitive TDPAC state characterized by a nuclear-spin quantum number I (in this case, the $I=5/2$ 482 KeV excited state of ^{181}Ta) and e is the proton's charge.

Pure hafnia, HfO_2, is monoclinic at room temperature. This phase is a distortion of the fluorite (CaF_2) structure. The unit cell has dimensions $a=5.1170_1$ Å, $b=5.1754_2$ Å, $c=5.2915_2$ Å, and $\beta=99.216_2$[26] and contains 12 atoms, four Hf, and eight O atoms at general positions of $C_{2h}^5(P2_1/c)$: $(4c) \pm (x,y,z;-x,y+1/2,1/2-z)$. x, y, and z are given in Table I. In this arrangement the Hf atoms exhibit a sevenfold-coordination with Hf-O bonds lengths between 2.04 and 2.26 Å. There are two kinds of oxygen atoms, which have different coordination: O(1) having three Hf neighbors between 2.04 and 2.15 Å and O(2) having four Hf between 2.16–2.26 Å. The shortest O-O distance is 2.52 Å.

As mentioned earlier, calculations were made for two Ta concentrations. First, substitution of one Hf atom by Ta in the 12-atoms unit cell; i.e., a Ta concentration of 25% ($Hf_{0.75}Ta_{0.25}O_2$) was considered. Then calculations were made for a periodic arrangement of 96-atoms supercells (SC), each constructed from eight unit cells of *m*-HfO_2. The resulting 96-atoms SC has dimensions $a'=2a=10.234$ Å, $b'=2b=10.3508$ Å, and $c'=2c=10.583$ Å and replacing a single Hf atom in the supercell by one Ta atom with an ordered compound, $Hf_{0.96875}Ta_{0.03125}O_2$, is simulated. It represents about 3 at. % doping. Additional calculations were performed (for some selected cases) using cells with 144 atoms ($a'=2a=10.234$ Å, $b'=2b=10.3508$ Å, and $c'=3c=15.8745$ Å), 192 atoms ($a'=2a=10.234$ Å, $b'=2b=10.3508$ Å, and $c'=4c=21.166$ Å), and 324 atoms ($a'=3a=15.351$ Å, $b'=3b=15.5262$ Å, and $c'=3c=15.8745$ Å), respectively. These additional calculations show that although a 3 at. % doping is large compared with parts per million (ppm) dilutions in the samples used in the TDPAC experiments, the choice of the 96-atoms SC keeps the Ta atoms sufficiently far from each other (10.3 Å) to avoid significant interactions. Differences smaller than 0.2×10^{21} V/m^2 were found in the principal EFG components when larger cells were considered. Regarding the structural properties, Ta-O nearest-neighbor bond lengths were unaltered (differences being smaller than the convergence error and the differences in the calculated forces between SCs smaller than 0.025 eV/Å) when larger SCs were considered. Thus, the 96-atoms SC is an excellent compromise between computational times and accuracy of the calculations.

The calculations were performed with the WIEN2K implementation[17] of the APW+LO method in a scalar relativistic version. Exchange and correlation effects were treated within density-functional theory using both the local-density approximation (LDA) (Ref. 27) and the generalized gradient approximation (GGA) (Ref. 28). For methodological purposes the unit cell is divided into nonoverlapping spheres with radius R_i and an interstitial region. The atomic spheres' radii used for Ta, Hf, and O were 1.06, 1.06, and 0.9 Å, respectively. The parameter $RK_{\max}$ controls the size of the basis set. Here R is the smallest muffin-tin radius and $K_{\max}$ the largest wave number of the basis set. $RK_{\max}$ is set to 8 for the 12-atoms cells and 6 for the 96-atoms SCs. The Hf and Ta-6*s*, 5*p* and 4*f*, and O-2*s* levels were included as *local orbitals*.[29] Once self-consistency of the potential was achieved, quantum-mechanically derived forces were obtained, the ions were displaced according to a Newton-damped scheme, and the new positions for the atoms were obtained (for details, see Ref 12). The procedure was repeated until the forces on the ions were below a tolerance value of 0.01 eV/Å. At each position the $V_{i,j}$ elements of the EFG tensor were obtained directly from the V_{LM} (angular momentum $L=2$) components of the lattice harmonic expansion of the Coulomb potential.[9,30] Integration in reciprocal space was performed using the tetrahedron method, taking an adequate number of k points in the first Brillouin zone.

III. STRUCTURAL AND ELECTRONIC PROPERTIES OF *m*-HfO_2

In order to check the reliability of the theoretical approach, it was applied to well established measured and previously calculated properties of pure bulk *m*-HfO_2. Therefore, before proceeding with the study of the doped system, a summary of the main results obtained for the pure system is given in this section.

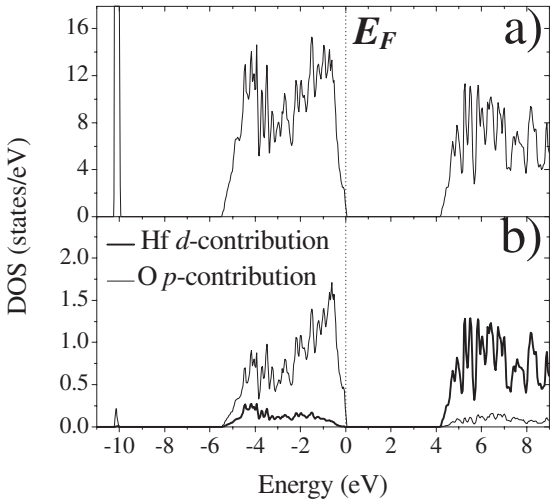

FIG. 1. (a) Total density of states of pure *m*-HfO_2 and (b) Hf *d* and O *p* partial DOS. Energies are referred to the valence-band maximum (labeled "E_F" here) shown by a vertical dotted line.

The lattice parameters were fixed at their experimental values, but the internal coordinates were optimized and the values are listed in Table I. As can be seen, the results obtained with both the LDA and GGA are very similar and in excellent agreement with experimental results[26,31] reported in the literature as well as previous calculation.[2–5] The density of states (DOS) of pure *m*-HfO_2 is shown in Fig. 1. The DOS and the overall band structure obtained here are consistent with previous theoretical results.[3–5,32] Both LDA and GGA functionals used in the APW calculations give an indirect band gap of about 4.1 eV [see Fig. 1(a)]. This calculated band is about 1.6 eV smaller than the measured gap, 5.68 eV.[32] This underestimation of the band gap, especially in metal oxides, reflects the well-known deficiency of LDA and GGA, but this does not invalidate the calculation of observables, which depend only on the ground state as, for example, the EFG and the atomic coordinates.

Figure 1(b) shows the DOS and the local DOS projected onto the Hf and O atoms. The total DOS is composed of two valence bands: a lower narrow band lying at about 10 eV below the Fermi level composed mainly by O 2*s* states and an upper band between-6.0 and 0.0 eV that has mainly O 2*p* character with a contribution of Hf 5*d* orbitals that evidence the covalent nature of the Hf-O bonds, in agreement with the picture of hafnia as an ionic insulator with some degree of covalent bonding between Hf and O atoms. The conduction band is a mixture of mainly Hf 5*d* and O 2*p* states. All these results are in agreement with previous theoretical studies and with photoemission and inverse photoemission results obtained from HfO_2 deposited on SiO_xN_y/p-Si, which showed that the valence band mainly has O 2*p* character while the conduction band mainly consists of Hf 5*d* states.[5,33]

The rest of this section describes the calculated EFGs at the Hf sites. Unfortunately, no Hf isotopes are used as probe in hyperfine techniques. For this reason, these results cannot

TABLE II. Largest component of the diagonalized EFG tensor (V_{ZZ}) and asymmetry parameter η at Hf sites in pure m-HfO_2. The calculations were performed using the experimental atomic positions (first row) and at the equilibrium positions predicted by the LDA and GGA calculations (second row). V_{ZZ} are in units of 10^{21} V/m^2.

	LDA calculation		GGA calculation	
	V_{ZZ}	η	V_{ZZ}	η
Experimental structural parameters	+11.6	0.53	+11.7	0.54
Predicted equilibrium structures	+12.6	0.11	+12.2	0.38

be compared with experimental data, but they can be used to study the differences originated by the substitution of an Hf atom by a Ta one in the EFG tensor. The EFGs were derived for two different sets of positions: the experimental coordinates and at those predicted by the calculations. These results are shown in Table II. It is important to note that LDA and GGA calculations performed here predict the same EFG when the experimental internal parameters x, y, and z are used, and it is concluded (due to the fact that the EFG is very sensitive to small changes in the electronic charge density) that the descriptions of the electronic structure predicted by these two calculations are very similar. In contrast to what has been observed in the case of the calculations performed using the experimental structural parameters, the results for the EFG obtained in the calculations performed at the equilibrium structures predicted by LDA and GGA calculations are different. There is a clear change in the symmetry of the EFG and a small decrease in magnitude going from LDA to GGA. This apparent discrepancy in the EFG values obtained by the two approximations used can be easily understood. In the case of the calculations performed at the experimental atomic positions (the calculations were performed with the same atomic positions), we have found similar EFGs in both calculations; but, in the case of the equilibrium structures, slightly different positions for the atoms were predicted. These results indicate that the different EFG values obtained in this case can be related to different equilibrium structures rather than the different descriptions of the electronic structure of the doped system. To support this assertion, a series of calculations was performed. (a) Using the equilibrium structure predicted by GGA an LDA calculation was made. In this case $V_{ZZ}=+12.0\times10^{21}$ V/m^2 and $\eta=0.39$ were found, almost identical to the results obtained by using the GGA parametrization ($V_{ZZ}=+12.2\times10^{21}$ V/m^2 and $\eta=0.38$). (b) Starting from a GGA calculation using the equilibrium positions predicted by LDA, it gave $V_{ZZ}=+12.5\times10^{21}$ V/m^2 and $\eta=0.10$, which is practically the same result as in the LDA calculation ($V_{ZZ}=+12.6\times10^{21}$ V/m^2 and $\eta=0.11$). From these tests it is concluded that, using the same structural positions, LDA and GGA predict the same EFG tensor. Then, the differences observed in Table II can be associated with the different equilibrium structures predicted in each calculation. A similar result was found for Cd in SnO.[21] These results are very interesting since small changes in the atomic positions produce large changes in the EFG tensor. This is a nice illustration of how the combination of hyperfine techniques and realistic calculations of the EFG may be used to obtain high precision structural refinements.

IV. Ta-DOPED m-HfO_2: RESULTS AND DISCUSSION

A. 12-atoms cell (Hf_3TaO_8)

After the study of undoped m-HfO_2, we have replaced a Hf atom by Ta in the cell, as described in Sec. II. As a first step, the self-consistent electronic structure of this system was calculated with all atoms in their initial unrelaxed positions in order to analyze the changes in the electronic structure of the system caused by the presence of the impurity, neglecting for the moment the problem of structural relaxations.

Pure m-HfO_2 is a wide band-gap semiconductor with the O p band filled and the Hf d band empty. Since the Ta valence is 5+, when a Ta atom replaces Hf, the resulting system is metallic, as can be seen in Fig. 2. Comparison of Figs. 1(a) and 2 shows that the presence of the Ta impurity induces an impurity band, partially filled at the bottom of the conduction band (indicated by arrows in Fig. 2 in the corresponding DOS). This band can be seen better looking at the band structure in this energy range as shown in Fig. 3. The band that is immediately above the Fermi level when crossing the A point corresponds to impurity states that are spatially located at Ta and at their oxygen nearest-neighbor (Onn) atoms. In particular, the impurity state has Ta d_{z^2} and Ta $d_{x^2-y^2}$ and Onn p_x, Onn p_y, and Onn p_z characters. Then, different charge states of the impurity are related with different symmetries of the electronic charge distribution in the neighborhood of the impurity. Therefore, as it was demonstrated in Refs. 11 and 12, the charge state of the impurity can modify the structural relaxations around the impurity and strongly affect the EFG. The question that arises here is the charge state of the impurity that corresponds to the experimental results. For this reason, calculations assuming two different physical situations were performed:

(i) It was assumed that a neutral Ta that substitutes Hf in m-HfO_2 remains in a +4 valence state. We will name this charge state "neutral charge state" ($q=0$). In this neutral charge state, as we show in Figs. 2 and 3, the impurity state located at the Fermi level is partially occupied.

(ii) In the real sample, the presence of defects (vacancies, interstitial atoms, and the presence of donor or acceptor impurities) or thermal effects can change the charge state of the impurity. In order to investigate this point, we have performed calculations removing ($q=+1$) one electron from the whole system. This impurity state is referred to as "charged state." As can be seen by comparing the results presented in Figs. 4(a) and 4(b), there is an almost "rigid band" behavior of the DOS where the removal of one electron has the only effect of making the impurity level at the top of the valence-band empty.

First, the EFG tensor was derived for unrelaxed atomic positions. As it was expected, the EFG strongly depends on the charge state of the impurity. In the case of LDA, we obtained $V_{ZZ}=2.2\times10^{21}$ V/m^2 and $\eta=0.38$ for $q=0$ and

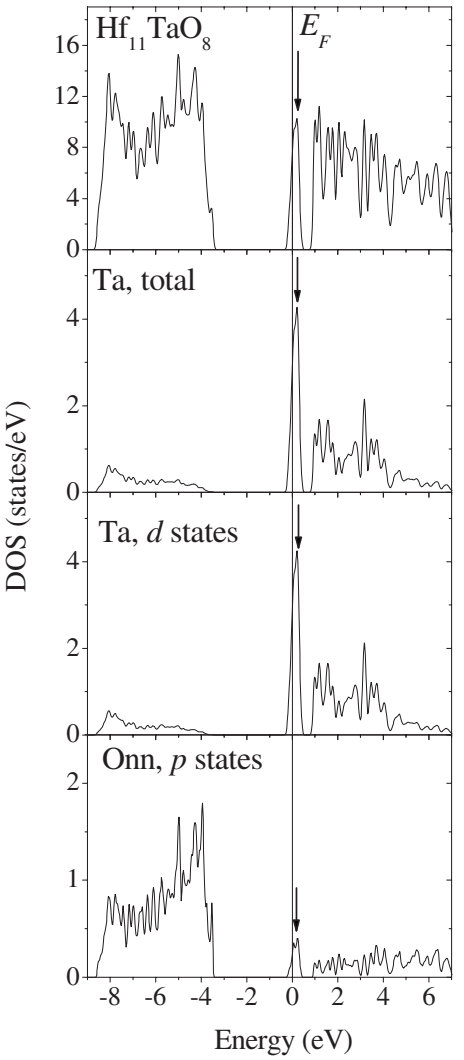

FIG. 2. Total DOS, atom-resolved Ta DOS, as well as Ta *d*, and one of its Onn *p*-DOS functions in Hf_3TaO_8 (unrelaxed structure). Energies are referred to the Fermi level (E_F). Similar results were found for the other Ta-Onn.

$V_{ZZ}=9.5\times10^{21}$ V/m^2 and $\eta=0.24$ for $q=1$. It is important to mention that LDA and GGA predict the same EFG for the unrelaxed structure. For both charge states, the EFGs at Ta sites are different from those corresponding to Hf sites in pure *m*-HfO_2 (see Table II). These differences in the EFGs illustrate the dominant electronic contribution to the EFGs arising from the different electronic structures of Hf and Ta at these sites.

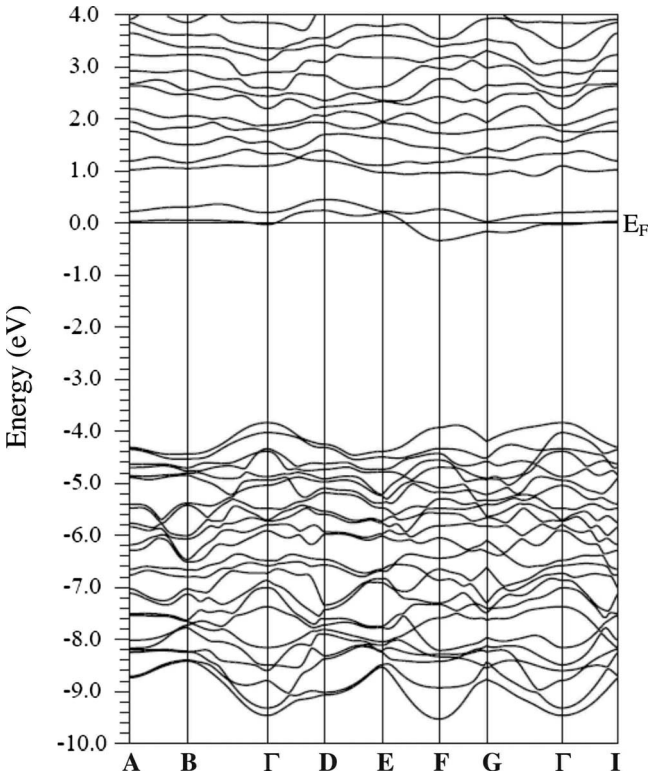

FIG. 3. Band structure for the system $TaHf_3O_8$ (unrelaxed). Zero energy is at the Fermi level (E_F).

The substitution of an Hf atom by a Ta impurity produces non-negligible forces on its nearest neighbors. In order to study the relaxation introduced by the impurity, we have considered the Ta and the Onn displacements until forces vanished. It was found that the amount of structural relaxation per atom decreases rapidly from the Onn to further shells, leading to minor changes in the positions of the Onn atoms. The EFG at the Ta site is essentially not affected by the relaxation of atoms lying beyond the Onn distance. In Table

TABLE III. Final distances of the Ta to its Onn for the different calculations performed with the 12-atoms cell and compared with the ones of pure *m*-HfO_2. *d*(Ta-Onn) are the distances (in Å) from Ta to each of its seven Onn atoms.

		$q=0$		$q=+1$	
d(Ta-Onn)	Unrelaxed structure	LDA	GGA	LDA	GGA
d(Ta-O1)	2.03	2.00	2.01	1.94	1.95
d(Ta-O2)	2.07	2.01	2.02	1.96	1.99
d(Ta-O3)	2.13	2.06	2.08	2.05	2.09
d(Ta-O4)	2.14	2.11	2.10	2.07	2.09
d(Ta-O5)	2.17	2.13	2.15	2.08	2.10
d(Ta-O6)	2.23	2.22	2.21	2.28	2.25
d(Ta-O7)	2.25	2.22	2.23	2.22	2.23

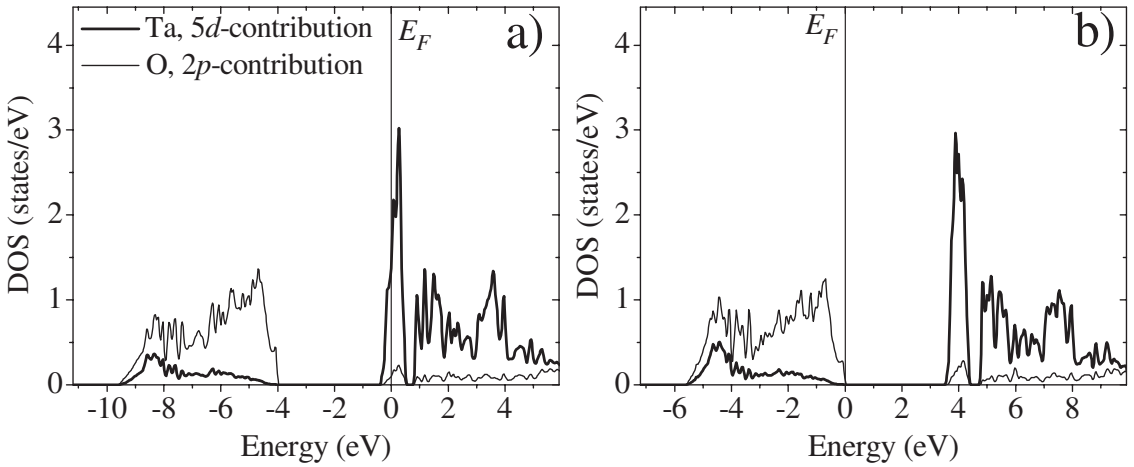

FIG. 4. Atom-resolved PDOS at Ta and its Onn atoms in the unrelaxed system $TaHf_3O_8$ for (a) $q=0$ and (b) $q=-1$. Energies are referred to the Fermi level (E_F) in (a) and the valence-band top in (b).

III the results of the relaxation of these oxygen atoms for the two charge states are compared. Additionally, it was found that the Ta impurity moved out from the symmetry site; but this displacement (0.03 Å for $q=0$ 0.01 Å in the case of $q=+1$) is very small compared to the displacement of the Ta-Onn. As can be seen in Table III, LDA and GGA predict almost the same structural distortions, the difference between the two approximations being smaller than 0.03 Å.

For both charge states, a contraction of the Ta-Onn bonds was found, but, as it was expected, the structural distortions strongly depend on the charge state of the impurity. As can be seen in Table III, the magnitude of the contractions is larger in the case of the charged impurity state. This is due to Coulomb interaction as was already observed in other doped oxides.[11,12,22] A similar result was found by Casali and Caravaca[24] using the *ab initio* all-electron new full-potential linear muffin-tin orbital method. Unfortunately, the authors give only the average contraction of the seven bond lengths with values of 4% and 5% for the neutral and charged cells, respectively. We have to mention here that these results were obtained in small supercells (24 and 48 atoms) and can be affected (as we will show in Sec. IV B) by size effects.

The contractions of the Ta-Onn bond lengths can be understood from the fact that the bond lengths in tantalum oxide (TaO_2) are about 2.02 Å. As in the case of Cd impurity substitutionally located at cationic sites in binary oxides (see Ref. 22 and references therein), it seems that the local structure tries to reconstruct the environment of Ta in its oxide. APW+LO calculations reported in Refs. 22 and 23 and calculations now in progress in Ta-doped binary oxides confirm this assertion.

In the following the APW+LO predictions for the EFG tensor will be discussed and compared with the experiments. Table IV contains the results for the major principal component and the asymmetry of the EFG tensor at Ta sites in the equilibrium structures and for the two charged states studied here. As can be seen, the resulting EFGs obtained with LDA and GGA are very similar. The difference in the EFGs obtained for the charged and neutral cells is remarkable and is not only caused by the different equilibrium structures obtained for each charge state. We will return to this point in Sec. IV B. Finally, the obtained predictions are in poor agreement with the experimental results.[34] We will see that this discrepancy is related to the high Ta concentration compared to that in the sample used in the experiment.

B. 96-atoms supercell ($Hf_{31}TaO_{64}$)

Section IV A presented the results obtained for Ta in m-HfO_2 using a small cell. The corresponding Ta concentra-

TABLE IV. Calculated principal EFG component, V_{ZZ}, in units of 10^{21} V/m^2 and asymmetry parameter η at the Ta impurity site in m-HfO_2 compared to experiment. The theoretical results were obtained with the relaxed structures for the two charge states considered. $Q=2.36_5$ b (Ref. 35) was used to calculate V_{ZZ} from the experimental quadrupole coupling constant ν_Q. The sign of the experimentally determined EFG is unknown.

		$q=0$		$q=+1$		
		LDA	GGA	LDA	GGA	Experimental result[a]
12 atoms cell (Hf_3TaO_8)	V_{ZZ}	+16.3	+16.9	+18.4	+18.7	$V_{ZZ}=13.7_1$
	η	0.30	0.32	0.10	0.10	$\eta=0.340_3$
96 atoms cell ($Hf_{31}TaO_{64}$)	V_{ZZ}	–	+21.2	–	+13.6	
	η	–	0.29	–	0.40	

[a]Reference 33.

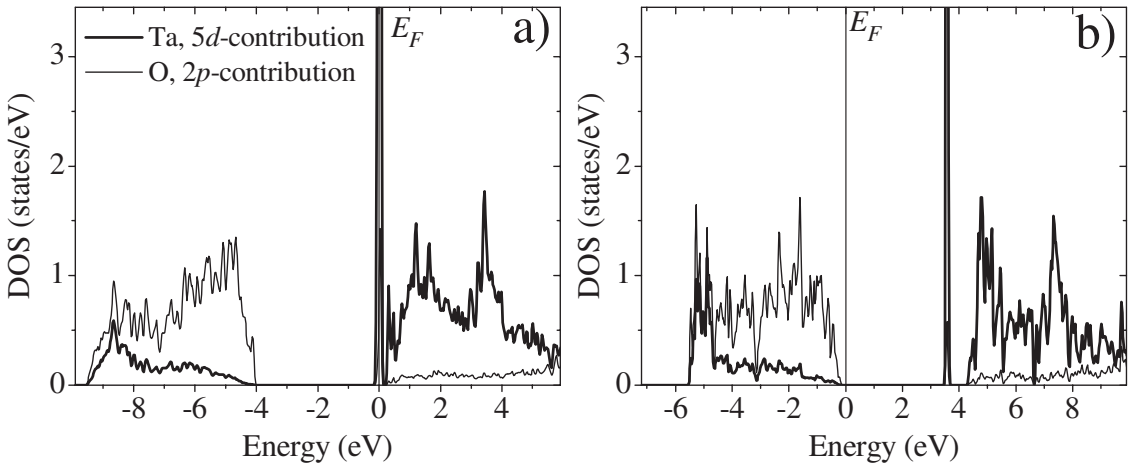

FIG. 5. Atom-resolved PDOS at Ta and its Onn atoms in the relaxed system $TaHf_{31}O_{64}$ for (a) $q=0$ and (b) $q=-1$. Energies are referred to the Fermi level (E_F).

tion is by far too high to allow a meaningful comparison with TDPAC experiments for dilute systems. The interaction between Ta neighbors cannot be neglected, and the structural relaxation of the Ta nearest neighbors can be constrained by this spurious interaction. Therefore calculations using a much larger supercell were performed. Again both the LDA and GGA were applied; but since the two approaches gave very similar results, only those obtained with GGA are included here.

Figures 5(a) and 5(b) present the DOS functions calculated for $Hf_{31}TaO_{64}$ for the two charge states studied. As can be seen, the Ta *d* band is described as very sharp peaks indicating that interaction between Ta atoms is quite small for this supercell. Table V contains the results for the relaxation of the seven nearest oxygen neighbors of the Ta impurity. For the two charge states, reductions in the Ta-Onn bond lengths were found. These results follow the tendency predicted in the previous calculation with a much smaller cell. Similar to the case of the 12-atoms cell, the structural distortion depends on the charge state of the impurity. Comparing the equilibrium Ta-bond lengths, Tables IV and V, it is seen that there are small differences between the equilibrium bond lengths predicted for the systems Hf_3TaO_8 and $Hf_{31}TaO_{64}$.

TABLE V. Final distances, *d*(Ta-Onn) (in Å), of Ta to its oxygen nearest neighbors for the two charge states calculated with the 96-atoms cell and compared with those of pure *m*-HfO_2 (GGA calculations).

	Unrelaxed structure	Relaxed structure	
d(Ta-Onn)		$q=0$	$q=+1$
d(Ta-O1)	2.03	2.01	1.97
d(Ta-O2)	2.07	2.03	1.98
d(Ta-O3)	2.13	2.10	2.06
d(Ta-O4)	2.14	2.08	2.08
d(Ta-O5)	2.17	2.14	2.08
d(Ta-O6)	2.23	2.17	2.15
d(Ta-O7)	2.25	2.21	2.18

These differences are larger than the convergence error bars, and it is concluded that the structural distortion induced by the Ta impurity depends on the impurity concentration. As the EFG generally decays as $1/r^3$, where *r* is a measure of distance from the producing charge density, it is particularly sensitive to slight local changes. For this reason, these small differences in the position of the Ta neighbors (especially the oxygen first neighbors) can strongly affect the EFG tensor.

In Table IV, the results for the EFG tensor at the Ta sites in equilibrium structures for the two charge states are given. Comparing the results obtained for the neutral cell for both Ta dilutions, there is a clear increase in the magnitude of V_{ZZ} going from the 12-atoms cell to the 96-atoms supercell and the asymmetry parameter changes from 0.32 to 0.29. In the case of the charged cell, the magnitude of V_{ZZ} decreases from 18.7×10^{21} to $+13.6\times10^{21}$ V/m^2 going from the 12-atoms cell to the 96-atoms supercell.

As discussed earlier, the EFG strongly depends on the Ta concentration. Since different concentrations produce different structural distortions, it is interesting to separate the electronic and structural effects. In order to do that, we have taken the 12-atoms cell and we fixed the Ta atom and its Onn at the equilibrium positions predicted for the system $Hf_{31}TaO_{64}$. At this position we calculated the EFG tensor at the Ta site. We obtain for the neutral cell ($q=0$) $V_{ZZ}=+11.5\times10^{21}$ V/m^2 and $\eta=0.47$. Besides the fact that the symmetry is similar to those found for the system $Hf_{31}TaO_{64}$ ($\eta=0.40$), the magnitude of V_{ZZ} is very different to those predicted for the large unit cell ($V_{ZZ}=+21.2\times10^{21}$ V/m^2, see Table IV). This calculation shows that there is a large Ta-Ta interaction in the case of the smaller cell that affects the structural relaxations and also the EFG when equal positions for the ions are considered. Similar conclusions were drawn in the case of the charged system.

The results obtained for the charged system agree very well (in magnitude and symmetry) (see Table IV) with the experimental results obtained for the EFG at Ta impurities substitutionally located at cationic sites in *m*-HfO_2. The difference between the EFGs obtained for the charged and neutral cells is very remarkable. The high value obtained for the magnitude of V_{ZZ} for $q=0$ implies, through a comparison

TABLE VI. p and d valence contributions to the electric-field gradient at Ta in m-HfO_2, in units of 10^{21} V/m^2, for the neutral and charged states of Ta in the system $Hf_{31}TaO_{64}$.

	$q=0$			$q=+1$		
	V_{ZZ}	V_{YY}	V_{XX}	V_{ZZ}	V_{YY}	V_{XX}
p	+8.9	−7.1	−1.8	+12.8	−8.8	−4.0
d	+15.3	−10.2	−5.1	+1.0	−1.0	0.0
s-d	+0.22	−0.18	−0.04	+0.22	−0.12	−0.10
Total valence	+24.5	−17.4	−7.06	+14.1	−10.0	−4.1

with experiment (performed at 300 K), that Ta is in a charged state when it is introduced as impurity in m-HfO_2 at room temperature. New experiments at very low temperatures could be very interesting in order to test our prediction for the EFG tensor corresponding to the neutral impurity, presuming this to be more abundant at low temperatures.

The EFG tensor is directly related to the anisotropy of the electronic density in the vicinity of the nucleus of the probe atom for which the EFG tensor is calculated or measured. The EFG can be decomposed into two contributions:[30] the first one is named the valence contribution since it originates from the nonspherical electron density of the valence (and semicore) electrons within the muffin-tin sphere. The second contribution is the lattice contribution originating from more distant regions of the crystal. In most cases (and also in the systems studied here), the valence contribution dominates, while the lattice term is almost negligible. For these reason, in order to investigate the origin of the difference in the EFG for the two charge states of the impurity, we concentrate on the valence contribution to the EFG. The dominant valence contribution can be further decomposed according to the different orbital symmetries. Table VI contains the total valence contribution to V_{ZZ} and its components arising from p and d and s-d orbital symmetries (higher l contributions are negligible). The largest differences are found for the d contributions to V_{ZZ}. The effect of the charge state of the impurity on the symmetry of the electronic charge density (and, in consequence, on the EFG tensor) can be seen in Figs. 6(a) and 6(b). In these figures we present the atom-resolved PDOS for the Ta atom in the relaxed 96-atoms supercell for both charge states of the impurity. As can be seen the impurity state at the Fermi level has an important Ta d_{z^2} and Ta $d_{x^2-y^2}$ contributions. These results show that even a small change in the population of an impurity state can induce a drastic change in the symmetry of the charge distribution and, in consequence, in the EFG tensor.

V. SUMMARY AND CONCLUSIONS

Density-functional calculations of electronic structures and atomic forces have been used to examine monoclinic HfO_2 in its pure form as well as with Ta impurities. The force calculations were used to optimize the defect structures, and from the self-consistent potentials electrical-field gradients were derived. This allowed a comparison to experimental results obtained by time-dependent perturbed angular correlation measurements. Only substitutional Ta impurities were considered, Ta replacing an Hf atom, and a supercell approach was employed; i.e., the defect hafnia was simulated by an ordered $Hf_{1-x}Ta_xO_2$ compound. Two Ta concentrations were chosen, $x=0.25$ and 0.03125 (96-atoms supercell, $Hf_{31}TaO_{64}$). Although the 3% Ta concentration is considerably larger than the Ta content in the samples used in the TDPAC experiments, it was shown, through test calculations with larger cells, that the 96-atoms supercell calculations yield results that are sufficiently size converged to allow comparison to the experimental data although the Ta concentration in the real samples are very low.

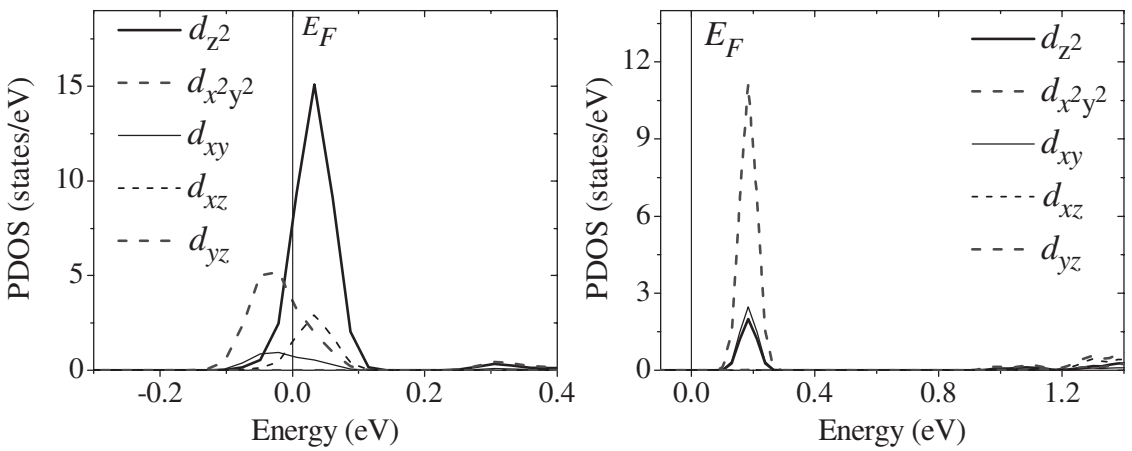

FIG. 6. Atom-resolved PDOS for Ta atom in the relaxed 96-atoms supercell for (a) the neutral charge state ($q=0$) and (b) the charged state ($q=+1$) of the impurity.

Similarly to what has previously been observed for other binary oxides, Ta introduces impurity levels in the band gap and induces significant structural distortions in the HfO_2 semiconductor host lattice. The structural relaxations as well as the EFGs depend on the charge state of the impurity. This dependence is very pronounced in the case of the EFG and was explained by analyzing the electronic structure of the defect hafnia. The difference in the EFG magnitude and symmetry between the charged and neutral states of the impurity arises because of the filling of the impurity level at the Fermi energy. These differences in the EFG tensors lead us to conclude, through a comparison with TDPAC experiment (performed at 300 K), that Ta occurs in a (+1) charged state when it is introduced as impurity in m-HfO_2 at room temperature. From these results we have confirmed that the EFG tensor is a very useful quantity because it is sensitive to subtle details of the electronic structure and can be determined experimentally with high resolution.

ACKNOWLEDGMENTS

This work was partially supported by Agencia Nacional de Promoción Científica y Tecnológica (ANPCyT) under Grant No. PICT98 03-03727, Consejo Nacional de Investigaciones Científicas y Técnicas (CONICET) under Grants No. PEI6174 and No. PIP6032, Fundación/Antorchas, Argentina, and the Third World Academy of Sciences (TWAS), Italy, under Grant No. RGA 97-057. This research made use of the HP-Parallel-Computing Bose Cluster and the computational facilities at IFLP and Departamento de Física (UNLP).

*Corresponding author.

[1] V. Fiorentini and G. Gulleri, Phys. Rev. Lett. **89**, 266101 (2002).
[2] A. S. Foster, F. Lopez Gejo, A. L. Shluger, and R. M. Nieminen, Phys. Rev. B **65**, 174117 (2002).
[3] J. Kang, E.-C. Lee, and K. J. Chang, Phys. Rev. B **68**, 054106 (2003).
[4] J. E. Jaffe, R. A. Bachorz, and M. Gutowski, Phys. Rev. B **72**, 144107 (2005).
[5] A. B. Mukhopadhyay, J. F. Sanz, and C. B. Musgrave, Phys. Rev. B **73**, 115330 (2006).
[6] B. H. Lee, L. Kang, R. Nieh, W.-J. Qi, and J. C. Lee, Appl. Phys. Lett. **76**, 1926 (2000); M. Gutowski, J. E. Jaffe, C.-L. Liu, M. Stoker, R. I. Hegde, R. S. Rai, and P. J. Tobin, *ibid.* **80**, 1897 (2002).
[7] M. Venkatesan, C. B. Fitzgerald, and J. M. D. Coey, Nature (London) **430**, 630 (2004).
[8] H. Weng and J. Dong, Phys. Rev. B **73**, 132410 (2006), and references therein.
[9] See, e.g., G. Schatz and A. Weidinger, *Nuclear Condensed Matter Physics—Nuclear Methods and Applications* (Wiley, Chichester, 1996); E. N. Kaufmann and R. J. Vianden, Rev. Mod. Phys. **51**, 161 (1979); H. Frauenfelder and R. M. Steffen, in *Alpha-, Beta-, and Gamma-Ray Spectroscopy*, edited by K. Siegbahn (North Holland, Amsterdam, 1966), Vol. 2.
[10] A. Lerf and T. Butz, Angew. Chem., Int. Ed. Engl. **26**, 110 (1987); T. Klas, J. Voigt, W. Keppner, R. Wesche, and G. Schatz, Phys. Rev. Lett. **57**, 1068 (1986); R. Vianden and U. Feuser, *ibid.* **61**, 1981 (1988); N. Achtziger and W. Witthuhn, Phys. Rev. B **47**, 6990 (1993); D. Lupascu, M. Uhrmacher, and K. P. Lieb, J. Phys.: Condens. Matter **6**, 10445 (1994); S. Lany, P. Blaha, J. Hamann, V. Ostheimer, H. Wolf, and T. Wichert, Phys. Rev. B **62**, R2259 (2000); J. Meersschaut, C. L'abbe, M. Rots, and S. D. Bader, Phys. Rev. Lett. **87**, 107201 (2001); L. A. Terrazos, H. M. Petrilli, M. Marszalek, H. Saitovich, P. R. J. Silva, P. Blaha, and K. Schwarz, Solid State Commun. **121**, 525 (2002); J. M. Ramallo-López, M. Rentería, E. E. Miró, F. G. Requejo, and A. Traverse, Phys. Rev. Lett. **91**, 108304 (2003); M. Forker, S. Müller, P. de la Presa, and A. F. Pasquevich, Phys. Rev. B **68**, 014409 (2003).
[11] L. A. Errico, G. Fabricius, M. Rentería, P. de la Presa, and M. Forker, Phys. Rev. Lett. **89**, 055503 (2002).
[12] L. A. Errico, G. Fabricius, and M. Rentería, Phys. Rev. B **67**, 144104 (2003).
[13] J. M. Adams and G. L. Catchen, Phys. Rev. B **50**, 1264 (1994).
[14] H. Akai, M. Akai, S. Blügel, B. Drittler, H. Ebert, K. Terakura, R. Zeller, and P. H. Dederichs, Prog. Theor. Phys. Suppl. **101**, 11 (1990).
[15] P. Hohenberg and W. Kohn, Phys. Rev. **136**, B864 (1964); W. Kohn and L. J. Sham, *ibid.* **140**, A1133 (1965).
[16] O. K. Andersen, Phys. Rev. B **12**, 3060 (1975).
[17] P. Blaha, K. Schwarz, G. K. H. Madsen, D. Kvasnicka, and J. Luitz, *WIEN2k: An Augmented Plane Wave Plus Local Orbitals Program for Calculating Crystal Properties* (Technische Universität, Wien, 2001).
[18] L. A. Errico, G. Fabricius, and M. Rentería, Hyperfine Interact. **136/137**, 749 (2001).
[19] L. A. Errico, M. Rentería, G. Fabricius, and G. N. Darriba, Hyperfine Interact. **158**, 63 (2004).
[20] L. A. Errico, M. Rentería, A. G. Bibiloni, and G. N. Darriba, Phys. Status Solidi C **2**, 3576 (2005).
[21] L. A. Errico, M. Rentería, and H. M. Petrilli, Phys. Rev. B **75**, 155209 (2007).
[22] L. A. Errico, G. Fabricius, and M. Rentería, Phys. Status Solidi B **241**, 2394 (2004).
[23] M. Rentería, G. N. Darriba, L. A. Errico, E. L. Muñoz, and P. D. Eversheim, Phys. Status Solidi B **242**, 1928 (2005).
[24] R. A. Casali and M. A. Caravaca, Solid State Commun. **134**, 413 (2005).
[25] P. Blaha, J. Phys.: Condens. Matter **3**, 9381 (1991).
[26] R. E. Hann, P. R. Suitchand, and J. L. Pentecost, J. Am. Ceram. Soc. **68**, C-285 (1985).
[27] J. P. Perdew and Y. Wang, Phys. Rev. B **45**, 13244 (1992).
[28] J. P. Perdew, K. Burke, and M. Ernzerhof, Phys. Rev. Lett. **77**, 3865 (1996).
[29] D. Singh, Phys. Rev. B **43**, 6388 (1991).
[30] P. Blaha, K. Schwarz, and P. H. Dederichs, Phys. Rev. B **37**, 2792 (1988); K. Schwarz, C. Ambrosch-Draxl, and P. Blaha, *ibid.* **42**, 2051 (1990).

[31] J. Wang, H. P. Li, and R. Stevens, J. Mater. Sci. **27**, 5397 (1992); D. M. Adams, S. Leonard, D. R. Russel, and R. J. Cernik, J. Phys. Chem. Solids **52**, 1181 (1991).
[32] M. Balog, M. Schieber, M. Michiman, and S. Patai, Thin Solid Films **41**, 247 (1977).
[33] S. Sayan, T. Emge, E. Garfunkel, X. Zhao, L. Wielunski, R. A. Bartynski, D. Vanderbilt, J. S. Suehle, S. Suzer, and M. Banaszak-Holl, J. Appl. Phys. **96**, 7485 (2004).
[34] A. Ayala, R. Alonso, and A. López-Garcia, Phys. Rev. B **50**, 3547 (1994).
[35] T. Butz and A. Lerf, Phys. Lett. **97**A, 217 (1983).